Synthesis and Characterization of Manganese Molybdate for Symmetric Capacitor Applications

Baskar Senthilkumar[1,2], Ramakrishnan Kalai Selvan[2], Danielle Meyrick[1] and Manickam Minakshi[1,]*

[1]School of Engineering and Information Technology, Murdoch University, Murdoch, WA 6150, Australia
[2]Solid State Ionics and Energy Devices Laboratory, Department of Physics, Bharathiyar University, Coimbatore 641 046, India
[*]E-mail: minakshi@murdoch.edu.au

A simple, one-step facile approach (precipitation technique) was employed to prepare manganese molybdate (α-MnMoO$_4$). The obtained powder was characterized by X-ray diffraction (XRD), Fourier Transform Infrared Spectroscopy (FT-IR) and scanning electron microscopy (SEM) for analyzing structural, functional group and morphological features. The formation of α phase MnMoO$_4$ particles was identified from XRD. The SEM results showed rhombohedral morphology of the particles. The capacitive behavior was investigated by cyclic voltammetry (CV), charge-discharge (CD) cycling and electrochemical impedance spectroscopy (EIS) studies using 2 M NaOH electrolyte at ambient atmosphere. From the cyclic voltammogram it was identified that the pseudocapacitance arises through the reversible faradic reactions of Mn^{3+}/Mn^{2+} ionic species. The α-MnMoO$_4$ electrode exhibited a capacitance of 200 F/g at a constant discharge current density of 1.6 A/g. The α-MnMoO$_4$ *vs.* α-MnMoO$_4$ symmetric supercapacitor device was fabricated and it delivered a maximum specific capacitance (81 F/g) with a specific energy density of 11 Wh/kg. The cycle life tests showed stable electrochemical performance up to 200 cycles with well rated cycle life and 1000 cycles providing 91 % of specific capacitance. The obtained values showed superior electrochemical performance than oxide counterparts.

1. INTRODUCTION

The electrochemical capacitor (EC) has attracted much attention in recent years as an alternative type of energy storage device, due to its high power density and reliability. Based on the charge storage mechanism, an EC can be classified as electrochemical double layer capacitors (EDLC)

or a 'pseudocapacitor'. The former stores charge in electric double layers at the electrode/electrolyte interface while the latter utilises both electric double layers and faradic processes to store energy. Supercapacitors are commonly used in regenerative braking mechanisms, pacemakers, electric vehicles, hybrid electric vehicles, forklifts and load cranes. In general, supercapacitors are used in high power applications due to their superior power density relative to batteries and their very high charge/discharge efficiencies. While currently used supercapacitors have a relatively low energy density compared to that of batteries they are nevertheless considered complementary devices to batteries, since they have high power density. Any improvement in the maximum specific capacitance will enhance their widespread exploitation in transport and electronic applications [1-3].

Usually, redox based supercapacitors (pseudocapacitor) provide a higher specific capacitance than that of EDLCs. This can be attributed to fast surface redox reactions. Electrode materials with a range of oxidation states for potential application in supercapacitors have been extensively studied, including RuO_2 [4], IrO_2 [5], MnO_2 [6], Fe_2O_3 [7], V_2O_5 [8], MoO_3 [9], $MnMoO_4/CoMoO_4$ [10] and $CoMoO_4$ [11]. Conducting polymers, including polyaniline (PANI) [12], polythiophene [13], poly(3,4-ethylenedioxythiophene) (PEDOT) [14] and its hybrid composites, PANI/TiO$_2$ [15], PANI/MnWO$_4$ [16], and PEDOT/NiFe$_2$O$_4$ [17] have also been investigated. Among the metal oxides mentioned, RuO_2 is a promising material that supplies high energy density (18.77 Wh/kg) [18] while exhibiting a maximum specific capacitance (SC) of 840 F/g [19]. Although RuO_2 demonstrates excellent electrochemical performance, its high cost and toxicity limits its commercialization. Identifying alternative low cost, non-toxic active materials is necessary for utilizing supercapacitors in a wide range of commercial applications.

The naturally abundant and environmentally benign manganese and molybdenum [9-11, 19-23] are chosen as potential electrodes for supercapacitor in this study. Simple MoO_2 [20] and MoO_3 [21] nanorods have previously been studied as electrodes for supercapacitors. These pure molybdenum oxide nanorods, MoO_2 and MoO_3, deliver very low specific capacitance (SCs) of 140 and 40 mF/g respectively. Composites of these materials, on the other hand, provide much higher capacitances. The highest capacitance of the composites thus far studied is yielded by PEDOT-MoO_3: 300 F/g compared to 40 mF/g for pure MoO_3 [22]. However, the molybdenum oxide composites are limited by poor cycling stability, low energy density and/or slow reaction kinetics [20-23]. To overcome these difficulties, Mai *et al.* [10] has prepared $MnMoO_4/CoMoO_4$ nanocomposites and heterostructured $MnMoO_4/CoMoO_4$ nanowires by micro-emulsion method and studied its detailed electrochemical analysis for supercapacitors. The reported SC for $MnMoO_4/CoMoO_4$ is 187 Fg^{-1} at a current density of 1 Ag^{-1} [10].

In our recent work on combustion synthesized $CoMoO_4$, $CoMoO_4.xH_2O$ and $NiMoO_4$ provided the SC of 90, 80 (for device) and 1116 Fg^{-1} (for a single cell) at 12 A/g respectively [24-25]. Liu *et al.* and Ghosh *et al.* reported cobalt and manganese molybdates [26-27] for capacitor applications but their chosen synthetic techniques were different and it is been tested for asymmetric device. Overall, the above mentioned works explored the suitability of metal molybdates ($MMoO_4$, M= Co and Ni) as electrode materials for supercapacitors.

In this work, we have prepared α-$MnMoO_4$ using a simple precipitation technique, and fabricated a $MnMoO_4$-based symmetric supercapacitor for the first time. The major objective of this

work is to attain improved capacitance through the use of a simple but novel synthetic procedure for manganese molybdate. Among the range of reported synthetic methods for $MnMoO_4$, including solid-state reaction [28], hydrothermal [27-29], liquid phase [30] and combustion syntheses [24, 31], precipitation is one of the most simple, low-cost, and environmental friendly methods. The physicochemical and electrochemical (capacitive) properties of precipitated α-$MnMoO_4$ are reported here.

2. EXPERIMENTAL METHODS AND MATERIALS

α-$MnMoO_4$ particles were synthesized by a simple precipitation technique using analytical grade pure manganese chloride tetrahydrate ($MnCl_2.4H_2O$), sodium molybdate ($Na_2MoO_4.2H_2O$) and sodium hydroxide (NaOH). Ten mmol of $MnCl_2.4H_2O$ and 10 mmol of $Na_2MoO_4.2H_2O$ were dissolved in 40 mL of double distilled water. The pH of the mixed solution was adjusted to pH 7 by the drop-wise addition of NaOH (2 M). After stirring for an hour, the precipitate was collected and washed with double distilled water. The sample, as prepared, was calcined at 600 ºC for 5 hours to form the single phase α-$MnMoO_4$. Powder X-ray diffractometer (Bruker, D8 advance) with CuKα radiation was used to identify the phase formed. Infrared absorption spectra were obtained in the 4000-400 cm^{-1} region using an FT-IR interferometer (Bruker). To investigate the morphology and elemental composition of the obtained α-$MnMoO_4$, Field Emission Scanning Electron Microscope (FESEM) (a Quanta 3D FEG) equipped with an energy dispersive X-ray spectrometer was used. The cyclic voltammetry, electrochemical impedance and galvanostatic charge/discharge studies of the samples were carried out using SP-150, Bio-Logic Science Instruments. The active electrode material was prepared by the suspension of $MnMoO_4$ (85 wt %), carbon black (10 wt %) and polyvinlidene fluoride (PVDF) (5 wt %) in 0.4 mL of N-methyl-2-pyrrolidinone (NMP) to form a slurry. An aliquot (10 µL) of slurry was coated on a graphite sheet (area of coating, 1 cm^2). An aqueous solution of 2 M of NaOH was used as the electrolyte. A platinum wire electrode and a saturated Ag/AgCl electrode were used as counter and reference electrodes, respectively. The α-$MnMoO_4$ symmetric two cell system having an equal mass loading was fabricated using polypropylene as the separator. The electrochemical studies were performed on both two and three electrode cell configurations.

3. RESULTS AND DISCUSSION

3.1. Physico-chemical characteristics of α-MnMoO₄

The XRD pattern of α-$MnMoO_4$ synthesized by precipitation technique is shown in figure 1. The observed diffraction peaks are in good agreement with the standard monoclinic α-$MnMoO_4$ (JCPDS card No. 01-072-0285) (Figure 1). The calculated lattice parameters, a = 10.5479 ± 0.0215 Å, b = 9.5480 ± 0.002 Å, c = 7.1346 ± 0.0054 Å, β = 106.3 ± 0.046° are consistent with the reported values [32] confirmed the formation of pure monoclinic α-$MnMoO_4$ phase with no detectable impurities. Moreover, the presence of the major (220) reflection in the X-ray diffractogram indicates

the presence of α-phase. Infrared spectroscopy was used to further investigate the phase purity and structural bonding related to the functional groups (inset: Figure 1). For the α-MnMoO$_4$ material, prominent absorption bands at 724, 799, 868 and 948 cm^{-1} are characteristic bands of tetrahedral MoO$_4$ groups [33] were observed, and their presence substantiates the formation of tetrahedral coordination of Mo on the surface of α-MnMoO$_4$.
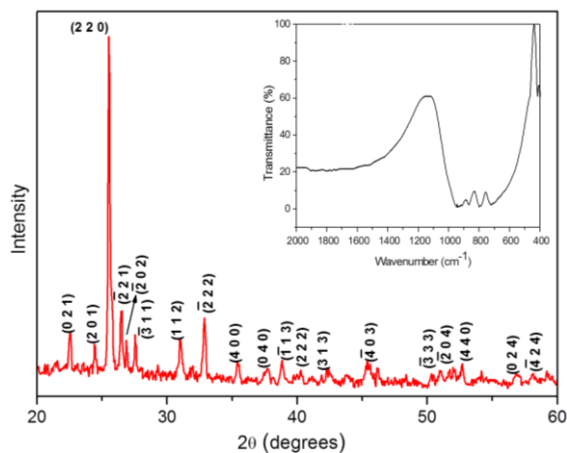

Figure 1. XRD pattern of α-MnMoO$_4$ powder (inset: FT-IR spectrum of α-MnMoO$_4$ powder).
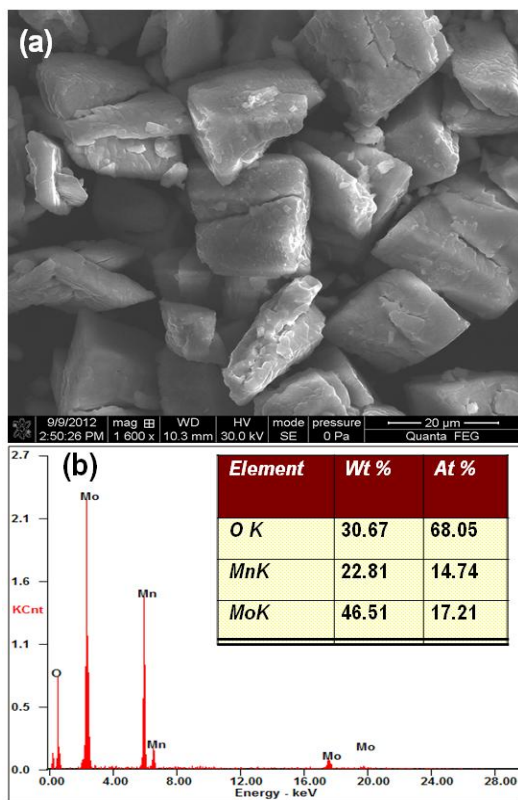

Figure 2. (a) FESEM image and (b) EDS spectrum of α-MnMoO$_4$ powder.

The bands at higher wavelengths represent symmetric MoO_4 stretching while the lower wavelengths correspond to asymmetric stretching [33]. The presence of the Mo=O group is also confirmed by the absorption band at the higher wavelength 948 cm^{-1}. The absence of any unassigned bands in the observed FT-IR spectrum further confirmed the phase purity of α-$MnMoO_4$. Scanning electron microscopy (SEM) (Figure 2 (a)) revealed rhombohedron-like morphology of the α-$MnMoO_4$ with a size range of 10 – 20 μm. A similar morphology was reported for $MnMoO_4$ prepared by the hydrothermal method [29]. The chemical compositions of the $MnMoO_4$ were evaluated using energy dispersive X-ray spectroscopy (EDS). The spectrum (Figure 2 (b)) shows strong peaks for Mn, Mo and O. No other detectable impurity peaks were observed confirming that substantiate washing has been done during the synthesis to remove sodium. The quantitative analysis of EDS showed the atomic ratio of 1:1:4 for elements Mn:Mo:O, illustrating the stoichiometric composition of $MnMoO_4$ is intact. Hence, the sample synthesized via this simple, single step precipitation method produced the required rhombohedron α-$MnMoO_4$.

3.2. Electrochemical properties of α-MnMoO₄

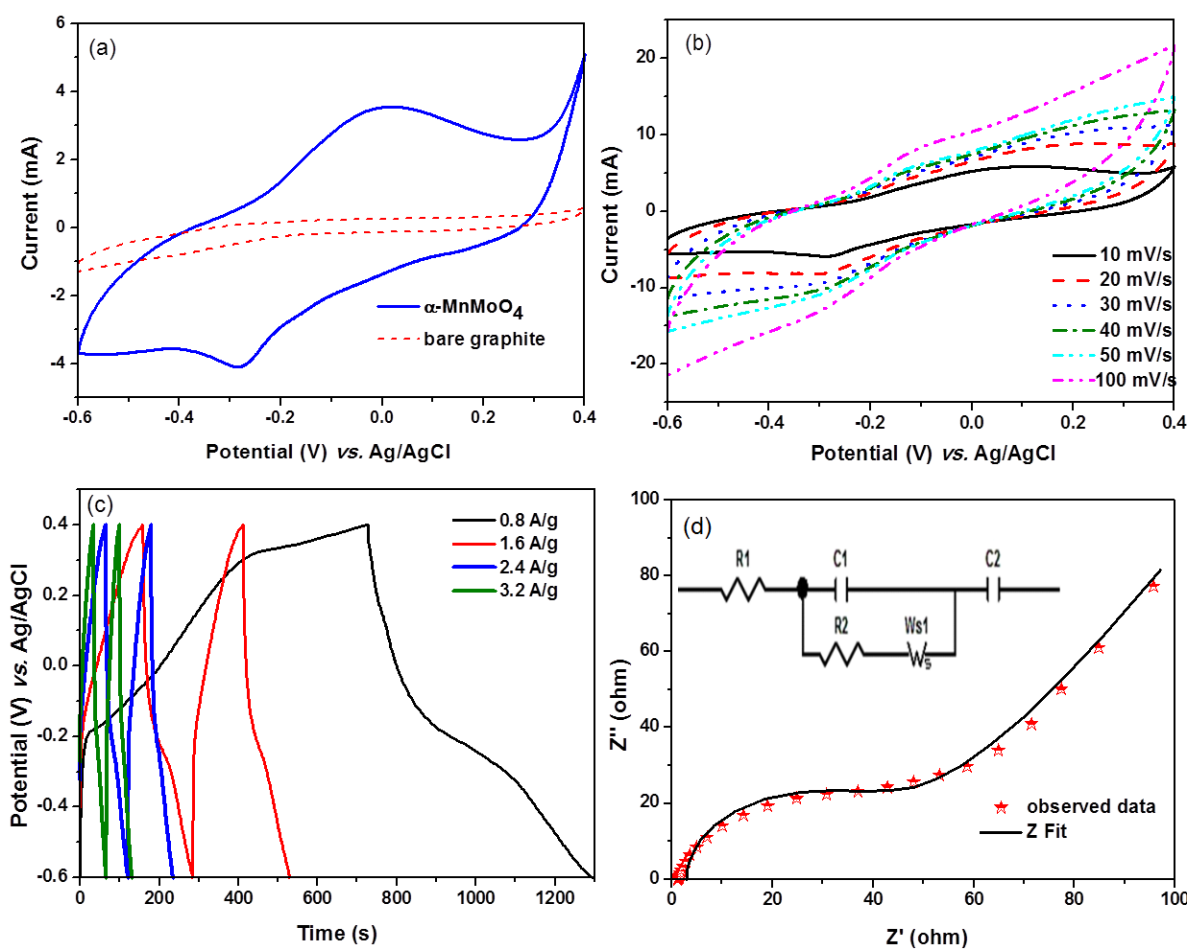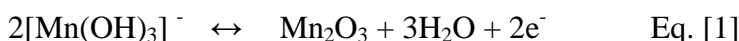**Figure 3.** (a) Cyclic voltammogram profile of α-$MnMoO_4$ and bare graphite as working electrodes at a scan rate of 5 mV/s. (b) Cyclic voltammogram profiles of α-$MnMoO_4$ at scan rates from 10 - 100 mV/s. (c) Galvanostatic charge-discharge curves of α-$MnMoO_4$ at a range of current densities. (d) Nyquist plot of the EIS of the α-$MnMoO_4$. The equivalent circuit diagram of different elements from the EIS analysis in shown in the inset.

The cyclic voltammogram of the synthesized α-MnMoO$_4$ as active working electrode against Pt wire as a counter is shown in Figure 3 (a). For the purpose of comparison, the first cycle of the electrode containing bare graphite is superimposed in the figure. The potential vs. current response of the cells was recorded over a potential range from -0.6 to 0.4 V *vs.* Ag/AgCl at a scan rate of 5 mV/s. No significant oxidation/reduction peak for the bare graphite electrode was evident. In addition, the magnitude of the area under the curve (measured current) for the bare graphite electrode is insignificant relative to that of the α-MnMoO$_4$ working electrode. This illustrates that the contribution to capacitance from bare graphite is negligible. For the α-MnMoO$_4$ electrode, a well defined oxidation and its corresponding reduction peak are observed at +0.015 and -0.281 V *vs.* Ag/AgCl. The reduction behavior of α-MnMoO$_4$ electrode infers pseudocapacitive behavior. The observed redox peaks in the potential range +0.015/-0.281V *vs.* Ag/AgCl for α-MnMoO$_4$ electrode are due to the faradic redox reaction shown in Eq. [1], which is identified from the Pourbaix diagram of Mn [10].

$$2[Mn(OH)_3]^- \leftrightarrow Mn_2O_3 + 3H_2O + 2e^- \qquad \text{Eq. [1]}$$

The voltammetric behavior of α-MnMoO$_4$ involves one electron (1e$^-$) transfer (Mn^{2+}/Mn^{3+}), corresponding to the fully reversible reaction shown in Eq. [1]. The derived specific capacitance is due to both the adsorption/desorption of electrolyte ions in the electrochemical double layer (EDLC) and the fast redox reactions on the surface of the active material [10, 21] corresponding to pseudocapacitance. Under the given experimental conditions (potential window, and pH of the electrolyte) it is suggested that the electrochemical reaction is limited to one electron transfer resulting in the formation of Mn$_2$O$_3$. The redox mechanism reported for this material in aqueous electrolyte [27] is quite similar to our studies shown in Fig. 3a.

Scan rates of 10, 20, 30, 40, 50 and 100 mV/s were employed (Figure 3b) to investigate the redox behavior of the electrode at higher scan rates. The size of the voltammogram increases by increasing the sweep rate. However, the shape and peak position deviates from the lower sweep rate. There is a linear increase in the peak current with the scan rate suggesting the electrode α-MnMoO$_4$ is suitable for high rate capability and demonstrates good reversibility [34]. The electrochemical activity of the working electrode (α-MnMoO$_4$) is found to be sustained for a far negative working potential (-0.6 V *vs.* Ag/AgCl), indicating that this material may also be used as an anode material for asymmetric supercapacitors [9].

The electrode was subjected to galvanostatic charge-discharge cycling in 2 M NaOH electrolyte at several current densities. The variation of the electrode potential during cycling is shown in Figure 3 (c) at a range of current densities. The observed quasi-symmetric charge-discharge profile again demonstrates the pseudocapacitive behavior. The calculated SC is 200, 134, 99 and 84 F/g at current densities of 1.6, 2.4, 3.2 and 6.4 A/g respectively. With an increase in current density, the SCs of individual electrode decreases due to an increase in ohmic drop (ionic resistivity) and incomplete material utilization [21, 35, 36]. The observed capacitance is high when compare with the reported MnMoO$_4$ (9.7 F/g at 1 A/g) and MnMoO$_4$/CoMoO$_4$ (187.1 F/g at 1 A/g) nanocomposite [10]. In general, the electrochemical capacitive performance of materials is largely influenced by its crystal structure, size, shape, morphology, surface area, porosity and electronic conductivity [37-41]. It is well documented that different structural phases yield different specific capacitances [37, 38]. In the present study we have prepared pure single phase α-MnMoO$_4$. It is certainly possible that the observed better

capacitance performance relative could be attributed to the purity of the phase. As well as the highly crystalline nature of the synthesized α-MnMoO$_4$ (calcined at 600 ^{o}C for 5 h) may enhance the charge carrier mobility, which would in turn enhance the capacitance [40, 41]. In addition, we have observed the well defined reversible peaks, which is well matched with the CV curves of combustion synthesized MnMoO$_4$ [26]. Similar type of redox peaks were observed for other metal molybdates also [11, 24-26].

Figure 3 (d) represents the electrochemical impedance spectrum (EIS) of α-MnMoO$_4$ recorded in open circuit potential at a frequency range of 10 kHz to 10 mHz with an applied potential amplitude of 10 mV. The EIS spectrum fitted with an equivalent circuit is shown in inset of Figure 3 (d). The Nyquist plot shows a single semicircle in the high frequency region and a linear spike inclination at 45° in the low frequency region. The semicircle represents double layer capacitance and the charge transfer resistance of the electrochemical system. The presence of the inclination may be attributed to diffusion of ions (mass transfer) near the electrode surface, illustrating the pseudocapacitive property of the α-MnMoO$_4$ material. The first intersection point of the semicircle in the high frequency region provides a value of solution resistance (R$_1$ = 1.2 Ω). The diameter of the semicircle represents the charge transfer resistance, (R$_2$ = 37.3 Ω) in the electrochemical system. The observed charge transfer resistance is comparable with the reported α-NiMoO$_4$ [26], and molybdenum oxides [42, 43]. Electrical double layer capacitance (C$_1$ = 3.989 mF) and pseudocapacitance (C$_2$ = 772 mF) were observed from EIS fitting. The EIS results substantiate the CV results; that is, that the maximum capacitance contribution of the material is based on fast surface redox reaction (pseudocapacitance).

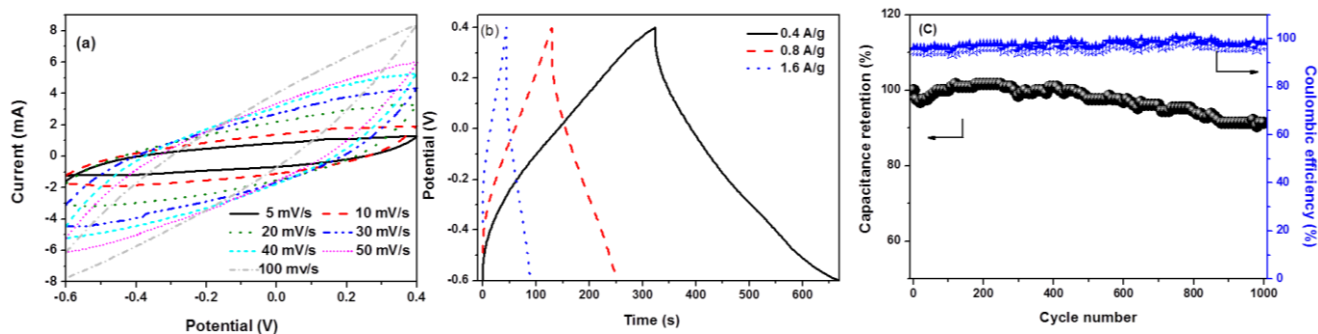### 3.3. Electrochemical performances of α-MnMoO$_4$ symmetric supercapacitor

Figure 4. (a) Cyclic voltammogram profiles of α-MnMoO$_4$ symmetric capacitor at at scan rates from 5 - 100 mV/s. (b) Galvanostatic charge-discharge curves of the α-MnMoO$_4$ symmetric capacitor at a various current densities. (c) Cycling and efficiency performance of α-MnMoO$_4$ symmetric capacitor at a current density of 0.8 A/g.

Figure 4 (a) shows the cyclic voltammogram of α-MnMoO$_4$ based symmetric supercapacitor at a range of scan rates (5 to 100 mV/s). The observed quasi-rectangular shape suggests good capacitive behavior. The anodic and cathodic current increased with increase in scan rate, illustrating a good rate capability of this material. The galvanostatic charge-discharge curve of the symmetric α-MnMoO$_4$ cell (Figure 4 (b)) showed a quasi-symmetric profile, further supporting good capacitive performance. IR

drop was observed due to the equivalent series resistance (ESR) of the cell. The specific capacitance of a single electrode was calculated [44] using the following equation (Eq. 2).

$$SC = I\,t/m\,\Delta V \qquad\qquad Eq.\quad [2]$$

Where, I is the current, m is the mass of the positive and negative electrode material, and t is the discharge time corresponding to the voltage window, ΔV. The SC of the α-MnMoO$_4$ symmetric cell is 81, 51 and 25 F/g at a current densities 0.5, 1 and 2 mA/cm^2 (0.4, 0.8 and 1.6 A/g), respectively. The α-MnMoO$_4$ symmetric capacitor delivers an energy density of 11 Wh/kg at a power density 100 W/kg. The SC of the sample decreased with increase in current density, due to the decrease in charge diffusion to inner active sites and the sluggish rate of redox reactions [35, 36]. This is reasonable to expect in pseudocapacitor in behavior of the α-MnMoO$_4$ material.

The cycle life of the cell was investigated up to 1000 cycles. Figure 4 (c) shows the stability of the SC and coulombic efficiency of the cell obtained at 1 mA/cm^2 tested for 1000 charge-discharge cycles. There is no significant capacitance fading up to 200 cycles; 91 % of initial capacitance of α-MnMoO$_4$ was retained even after 1000 cycles. A high coulombic efficiency ($>$ 95%) was observed for the α-MnMoO$_4$ symmetric cell. These studies suggest that α-MnMoO$_4$ synthesized via a simple precipitation method demonstrates good cycling stability and better reversibility than MoO$_2$ for the fabrication of redox supercapacitors.

4. CONCLUSIONS

In the present work, α-MnMoO$_4$ particles have been successfully prepared by a precipitation method. The combination of both adsorption/desorption processes (EDLC) and fast surface redox reactions (pseudocapacitance) in the α-MnMoO$_4$ material exhibit excellent electrochemical properties that led to high capacitive behavior with long term stability. Higher specific capacitance (81 F/g) and energy density (11 Wh/kg) were delivered by α-MnMoO$_4$ symmetric capacitor. The cycling stability of the capacitor was tested and 91% of initial capacitance was retained after 1000 cycles. The α-MnMoO$_4$ was found to be a suitable electrode material for redox supercapacitors.

References

1. B.E. Conway, Electrochemical Supercapacitors: Scientific Fundamentals and Technological Applications. Kluwer Academic: New York, 1999.
2. P. Simon, Y. Gogotsi, *Nat. Mater.* 7 (2008) 845.
3. G. Wang, L. Zhang, J. Zhang, *Chem. Soc. Rev.* 41 (2012) 797.
4. A. Devadas, S. Baranton, T. W. Napporn, C. Coutanceau, *J. Power Sources* 196 (2011) 4044.
5. Y. M. Chen, J. H. Cai, Y. S. Huang, K. Y. Lee, D. S. Tsai, *Nanotechnology* 22 (2011) 115706.
6. W. Wei, X. Cui, W. Chen, D. G. Ivey, *J. Power Sources* 186 (2009) 543.
7. K. Xie, J. Li, Y. Lai, W. Lu, Z. Zhang, Y. Liu, L. Zhou, H. Huang, *Electrochem. Commun.* 13 (2011) 657.
8. G. Wee, H. Z. Soh, Y. L. Cheah, S. G. Mhaisalkar, M. Srinivasan, *J. Mater. Chem.* 20 (2010) 6720.
9. W. Tang, L. Liu, S. Tian, L. Li, Y. Yue, Y. Wu, K. Zhu, *Chem. Commun.* 47 (2011) 10058.
10. L-Q. Mai, F. Yang, Y-L. Zhao, X. Xu, L. Xu, Y-Z. Luo, *Nat. Commun.* 2 (2011) 381.

11. Z. Xu, Z. Li, X. Tan, C. M. B. Holt, L. Zhang, B. S. Amirkhiz, D. Mitlin, *RSC Adv.* 2 (2012) 2753.
12. V. S. Jamadade, D. S. Dhawale, C. D. Lokhande, *Synth. Met.* 160 (2010) 955.
13. B. Senthilkumar, A. Thenamirtham, R. Kalai Selvan, *Appl. Surf. Sci.* 257 (2011) 9063.
14. S. Patra, N. Munichandraiah, *J. Appl. Polym. Sci.* 106 (2007) 1160.
15. K. Xie, J. Li, Y. Lai, Z. Zhang, Y. Liu, G. Zhang, H. Huang, *Nanoscale* 3 (2011) 2202.
16. S. Saranya, R. Kalai Selvan, N. Priyadharsini, *Appl. Surf. Sci.* 258 (2012) 4881.
17. P. Sen, A. De, *Electrochim. Acta* 55 (2010) 4677.
18. H. Xia, S. Meng, G. Yuan, C. Cui, L. Lu, *Electrochem. Solid -State Lett*. 15 (2012) A60.
19. W. Sugimoto, H. Iwata, Y. Yasunaga, Y. Murakami, Y. Takasu, *Angew. Chem. Int. Ed.* 42 (2003) 4092.
20. J. Rajeswari, P. S. kishore, B. Viswanathan, T. K. Varadarajan, *Electrochem. Commun*. 11 (2009) 572.
21. I. Shakir, M. Shahid, H. W. Yang, D. J. Kang, *Electrochim. Acta* 56 (2010) 376.
22. A. V. Murugan, A. K. Viswanath, C. S. Gopinath, K. Vijayamohanan*, J. Appl. Phys.* 100 (2009) 074319.
23. I. Shakir, M. Shahid, S. Cherevko, C-H. Chung, D. J. Kang, *Electrochim. Acta* 58 (2011) 76.
24. S. Baskar, D. Meyrick, R. Kalai Selvan and M. Minakshi, *Chem. Engineering Journal* 253 (2014) 502.
25. S. Baskar, D. Meyrick, Y.-S. Lee, and R. Kalai Selvan, *RSC Adv.* 3 (2013) 16542.
26. M-C. Liu, L-B. Kong, C. Lu, X-J. Ma, X-M. Li, Y-C. LuO, L. Kang, *J. Mater. Chem. A* 1 (2013) 1380.
27. D. Ghosh, S. Giri, Md. Moniruzzaman, T. Basu, M. Mandal and C. K. Das, *Dalton Trans*. 43 (2014) 11067.
28. S-S. Kim, S. Ogura, H. Ikuta, Y. Uchimoto, M. Wakihara, *Solid State Ionics* 146 (2002) 249.
29. Y. Ding, Y. Wan, Y. L. Min, W. Zhang, S. H. Yu, *Inorg. Chem.* 47 (2008) 7813.
30. B. Hu, X. Kang, W. Chen, F. Yang, S. Hu*, Cryst. Eng. Commun.* 13 (2011) 1755.
31. C. Sekar, R. Kalai Selvan, S. T. Senthilkumar, B. Senthilkumar, C. Sanjeeviraja, *Powder Technology* 215-216 (2012) 98.
32. S. Lei, K. Tang, Q. Liu, Z. Fang, Q. Yang, H. Zheng, *J. Mater. Sci.* 41 (2006) 4737.
33. A. Clearfield, A. Moini, P. R. Rudolf, *Inorg. Chem.* 24 (1985) 4606.
34. J. Li, M. Cui, Y. Lai, Z. Zhang, J. Fang, Y. Liu, *Synth. Met.* 160 (2010) 1228.
35. C-C. Hu, E. Chen, J-Y. Lin, *Electrochim. Acta* 47 (2002) 2741.
36. T. Morishita, Y. Soneda, H. Hatori, M. Inagaki, *Electrochim. Acta* 52 (2007) 2478.
37. S. Devaraj, N. Munichandraiah, *J. Phys. Chem. C* 112 (2008) 4406.
38. T. Brousse, M. Toupin, R. Dugas, L. Athouel, O. Crosnier, D. Belanger, *J. Electrochem. Soc.* 153 (2006) A2171.
39. P. Yu, X. Zhang, Y. Chen, Y. Ma, *Mater. Lett*. 64 (2010) 61.
40. R. Kalai Selvan, I. Perelshtein, N. Perkas, A. Gedankan*, J. Phys. Chem. C* 112 (2008) 1825.
41. K. Vijaya Sankar, D. Kalpana, R. K. Selvan, *J. Appl. Electrochem.* 42 (2012) 463.
42. H. Farsi, F. Gobal, H. Raissi, S. Moghiminia, *J. Solid State Electrochem.* 14 (2010) 643.
43. X. Xia, Q. Hao, W. Lei, W. Wang, H. Wang, X. Wang, *J. Mater. Chem*. 22 (2012) 8314.
44. G.P. Pandey, A.C.Rastogi, C.R.Westgate, *J. Power Sources* 245 (2014) 857.